A R C H I V E S O F M E T A L L U R G Y A N D M A T E R I A L S
Volume 60 2015 Issue 2
DOI: 10.1515/amm-2015-0106

HA-RIM AN*, HYELAN AN*, DOH-HYUNG RIU*,**, HYO-JIN AHN*,♯

IMPROVED PHOTOVOLTAIC PROPERTIES OF DYE-SENSITIZED SOLAR CELLS USING LASER PATTERNED F-DOPED SnO_2 THIN FILMS

POPRAWA WŁAŚCIWOŚCI FOTOWOLTAICZNYCH OGNIW SŁONECZNYCH UCZULONYCH BARWNIKIEM PRZEZ LASEROWĄ MODYFIKACJĘ POWIERZCHNI CIENKICH WARSTW SnO_2

We modified the surfaces of F-doped SnO_2 thin films using laser patterning to improve the photovoltaic properties of dye-sensitized solar cells. To do so, we varied the laser power density and the distance between laser-patterned lines. First, we investigated three power densities. Higher densities led to higher sheet resistances owing to increases in surface roughnesses. The lowest power density increased surface roughness without electrical degradation. Next, we explored three line spacings at a fixed power density. The films with the narrowest spacing exhibited the highest power conversion efficiency (~7.00%), the highest short-circuit photocurrent density (16.28 mA/cm^2), and a good fill factor (58.82%).

Keywords: Dye-sensitized solar cells · F-doped SnO_2 thin films · Surface morphology · Laser patterning

1. Introduction

Transparent conductive oxides (TCOs) have been widely used in the optoelectronics industry as essential components in flat panel displays, smart windows, gas sensors, light emitting diodes, and solar cells [1-3]. For indusitrial uses, TCOs must simultaneously possess both low electrical resistivities (ρ <$10^{-4}\Omega\cdot$ cm) and high optical transmittances (>80% at 550 nm) [4,5]. In general, TCOs can be classified as either n-type or p-type TCOs, depending on the type of dopants. Most currently used TCO materials are n-type semiconductors, such as Cd, In, Sn, Zn, and Ga-based oxides, because p-type TCOs show low carrier mobilities owing to the large effective masses of holes [6]. Among the various n-type TCOs, F-doped SnO_2 (FTO), which is commonly used in dye-sensitized solar cells (DSSCs), is a promising material because of its chemical stability, high temperature resistance, and high mechanical hardness, as well as its excellent electrical and optical properties [7,8]. DSSCs, which are composed of working electrodes covered with porous layers of TiO_2 particles and counter electrodes coated with Pt catalysts, require transparent FTO thin films to act as charge collectors [9]. However, there are some problems with DSSCs, such as the high costs of Ru-based dyes and Pt catalysts, the low durabilities of such dyes, the low stabilities of liquid electrolytes, and losses of photoinjected electrons at the interfaces between the dye-bonded TiO_2 layer on the FTO thin films and the electrolyte. With regard to the above-mentioned problems, one strategy being used to reduce the loss of photoelectrons at the interface between the dye-bonded TiO_2 layer on the FTO thin films and the electrolyte is to modify the surfaces of the FTO thin films [10,11]. Generally, the methods used for modifying the surfaces of FTO thin films are surface treatments using $TiCl_4$ solutions and direct surface etching techniques, such as reactive ion etching (RIE), inductively coupled plasma (ICP) etching, and laser patterning [12-15]. For example, Zou *et al.* studied the effects of $TiCl_4$ treatments on the photovoltaic parameters, including short-circuit current density and fill factor, of DSSCs. The $TiCl_4$ treatment produced FTO thin film layers with larger surface areas, leading to better performing DSSCs since they can absorb much more dye [13]. Further, Wang *et al.* carried out FTO surface modification by RIE using nanoimplant lithography. DSSCs fabricated with etched FTO thin films exhibited higher performances, compared to DSSCs fabricated with nonetched FTO thin films, because of the enhanced fill factors and power conversion efficiencies of the former [12]. Of the above-mentioned methods, laser patterning is a popular process for etching TCO films for use in various applications because it exhibits several advantages: there is no contact between the tools and the work pieces. Thus, there is little chipping. Further, it is fast and highly accurate [15,16]. Until now, the relationships between the laser patterning parameters and the photovoltaic performance of DSSCs have not clarified. In this study, we investigated the effects of the laser power density and the distances between laser-patterned lines on the photovoltaic properties of DSSCs.

* DEPARTMENT OF MATERIALS SCIENCE AND ENGINEERING, SEOUL NATIONAL UNIVERSITY OF SCIENCE AND TECHNOLOGY, SEOUL 139-743, KOREA
** RESEARCH INSTITUTE OF SOLAR CERAMIC, SOLAR CERAMIC CO., LTD., SEOUL 153-801, KOREA
♯ Corresponding author: hjahn@seoultech.ac.kr

2. Experimental

A laser patterning procedure was used to modify the surface morphologies of FTO thin films (6.97 Ω/p). Before being laser patterned, the FTO thin films were successively cleaned in ultrasonic baths with acetone, ethyl alcohol, and de-ionized (DI) water and then dried using an air blower. For laser patterning, a Nd:YAG laser (KORTherm Science, 355 nm, 10 W), able to etch surfaces at various wavelengths and output powers, was employed. To investigate the effect of the surface morphology of the FTO thin films on DSSC performance, we adjusted two parameters: the laser power density (power densities of 3320, 2400, and 1100 kW/mm^2 were used; the corresponding samples are referred to as samples A, B, and C, respectively) and the distances between the patterned lines (distances of 500, 250, and 130 μm were used; the corresponding samples are referred to as samples C, D, and E, respectively). The laser-patterned FTO thin films were used as current collectors in the working electrodes of DSSCs. To produce the working electrodes, pastes of inks were fabricated by grinding ink mixture consisting of P25 (Degussa), hydroxypropyl cellulose (HPC,M_w = ~80,000 g/mol, Aldrich), acetyl acetone (Aldrich), and DI water in an agate mortar. Next, the laser-patterned FTO thin films were squeeze printed using the ink pastes and annealed at 500°C for 1 h. Next, they were immersed in a solution of N719 (Ru(dcbpy)$_2$(NCS)$_2$, Solaronix) in ethanol for 24 h. A 0.6 M BMII (1-butyl-3-methylimidazolium iodide)-based iodine solution was used as the electrolyte in the DSSCs. For the counter electrode, nonpatterned FTO thin films were spin coated with a 5mM solution of chloroplatinic acid hydrate ($H_2PtCl{\cdot}xH_2O$, Aldrich) in 2-propanol and annealed at 450°C for 0.5 h.

To examine the effects of the power density and interline distance on the surface morphologies and roughnesses of the FTO thin films, field-emission scanning electron microscopy (FESEM, Hitachi S-4700) and atomic force microscopy (AFM, diDimension^{TM} 3100) were used. The electrical and optical properties of the laser-patterned FTO thin films were characterized using a Hall effect measurement system (Ecopia, HMS-3000) and a ultraviolet-visible (UV-vis) spectrophotometer (Scinco, S-3100), respectively. The photovoltaic properties of the DSSCs were measured using a solar simulator (McScience, K101 LAB20) equipped a 150 W xenon lamp and having a light intensity of 100 mA/cm^2.

3. Results and discussion

Figures 1 (a-b), (d-e), and (g-h) show top-view FESEM images of samples A-C etched at the three different laser power densities. The distances between the patterned lines of samples A-C were fixed at ~500 μm. As the laser power density was increased, the widths and depths of the patterned lines tended to increase as well. The widths of the patterned lines were ~22 μm for sample A, ~18 μm for sample B, and ~15 μm for sample C. In addition, the lines of samples A and B were connected continuously at the higher laser power density. However, in the case of sample C, the lines consisted of disconnected dots when the laser power density was low, as shown in Figure 1(h). Figures 1 (c), (f), and (i) show cross-sectional FESEM images of samples A-C. The depths of the patterned lines were ~476, ~380, and ~219 nm for samples A, B, and C, respectively. This indicates that the depth of the patterned lines was directly related to the laser power density. That is to say, higher laser power densities produced deeper patterned lines. These FESEM results indicate that the laser power density strongly affects the electrical properties of FTO thin films, and therefore the performance of the DSSCs based on the films.

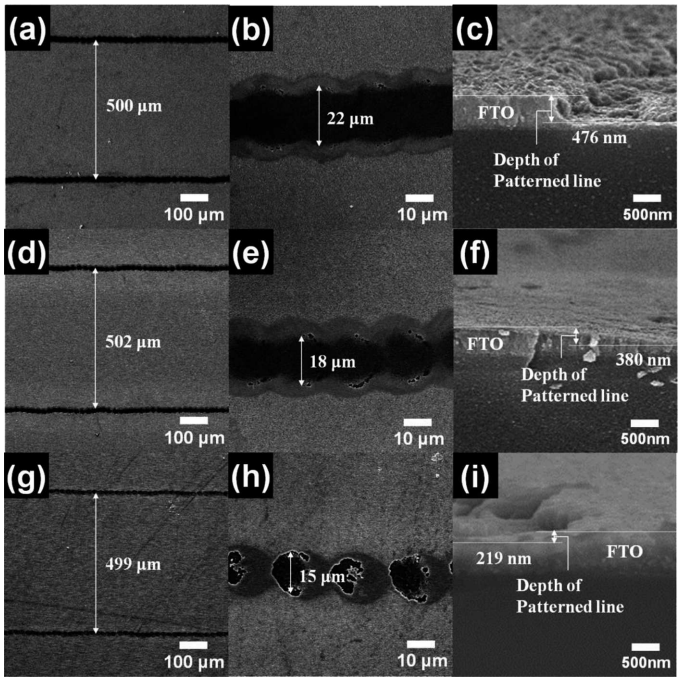

Fig. 1. Top-view and cross-sectional FESEM images of sample A (a-c), sample B (d-f), and sample C (g-i)

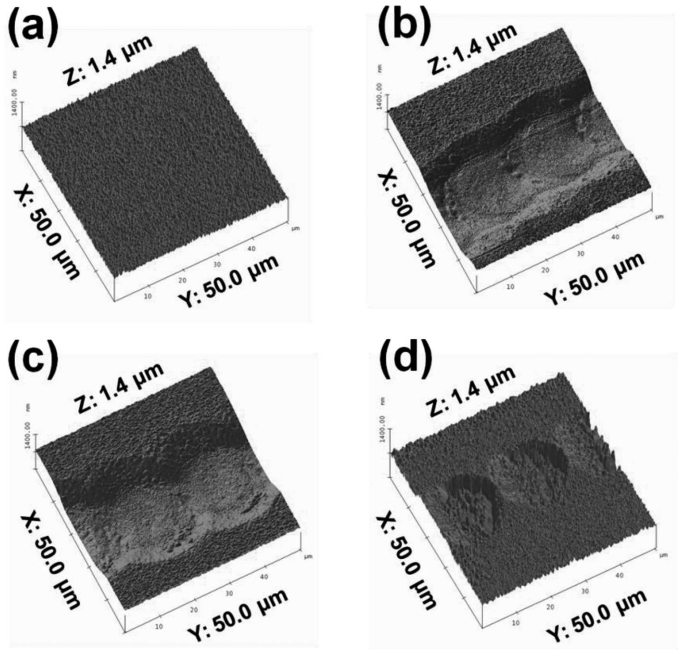

Fig. 2. AFM images of the nonpatterned FTO thin film (a), sample A (b), sample B (c), and sample C (d)

To investigate further the surface roughnesses of the samples laser-patterned using different laser power densities, AFM

was performed; the resultant images are shown in Figures 2 (a)-(d). The root mean square (RMS) roughness values for samples A, B, and C were ~313.3, ~219.5, and ~92.7 nm, respectively. Compared to nonpatterned FTO thin film (~26.6 nm), all the samples were considerably rougher. That implies that, as the laser power density was increased, the surface roughnesses of the laser-patterned FTO thin films increased, because of the wider and deeper patterned lines produced. Therefore, these results agree well with the FESEM images.

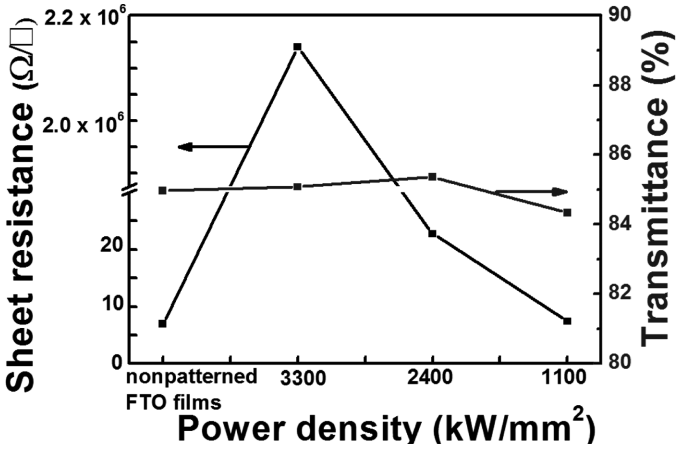

Fig. 3. Sheet resistances and optical transmissions at 550 nm of the samples depending on the laser power densities

TABLE 1
List of sheet resistances and transmittances of samples A-E and the nonpatterned FTO thin films

Samples	Sheet resistance (Ω/ף)	Transmittance (%, 550nm)
Non-patterned FTO thin films	6.97	84.96
Sample A	2.14×10^6	85.08
Sample B	22.79	85.36
Sample C	7.42	84.33
Sample D	7.76	83.73
Sample E	7.86	83.39

Figure 3 and Table 1 show the electrical and optical properties of samples A-C, which were etched at the various laser power densities. While the sheet resistance of nonpatterned FTO thin film was 6.97 Ω/ף, sample A showed the highest sheet resistance (2.14×10^6 Ω/ף). That is to say, sample A, which was patterned using the highest laser power density, exhibited the poorest electrical properties. This is because using a higher laser power density when patterning increases the depth of the patterned lines, disturbing the smooth transfer of electrons along FTO surface. However, the depths of the patterned lines decreased as the laser power density was decreased. Thus, the sheet resistances decreased drastically, to 22.79 Ω/ף for sample B and 7.42 Ω/ף for sample C. In particular, sample C exhibited electrical properties similar to those of the nonpatterned FTO thin film. That is to say, sample C exhibited high surface roughness without showing a decrease in its electrical conductivity. The optical transmittances of all the samples at 550 nm are shown in Figure 3. After the laser patterning of the FTO thin film, all samples demonstrated a constant transmittance of approximately 84%. This result demonstrates that laser patterning has little impact on the optical properties of FTO thin films.

TABLE 2
List of photovoltaic parameters of samples A-E with the nonpatterned FTO thin films

Samples	Open circuit voltage (V_{oc}, V)	Photocurrent density (J_{sc}, mA/cm^2)	Fill factor (FF, %)	Power conversion efficiency (PCE, %)
Non-patterned FTO thin films	0.74	13.01	65.95	6.29
Sample A	0.74	6.35	36.99	1.72
Sample B	0.74	11.45	40.30	3.43
Sample C	0.74	15.02	59.46	6.58
Sample D	0.73	15.83	59.66	6.84
Sample E	0.73	16.28	58.82	7.00

To investigate the photovoltaic properties of the laser-patterned FTO thin films, the solar simulator was employed. The photocurrent density-voltage (J-V) curves and photovoltaic parameters of DSSCs based on the different samples are shown in Figure 6 and Table 2. The power conversion efficiency (PCE, η) of the samples was calculated using the following equation [17]:

$$\eta\,(\%) = \frac{[J_{SC} \times V_{OC} \times ff]}{[I_{max} \times V_{max}]} \tag{1}$$

where J_{sc} is the short-circuit photocurrent density, V_{oc} is the open-circuit voltage, ff is the fill factor, I_{max} is the maximum power current, and V_{max} is the maximum power voltage. These patterned FTO thin films were used as current collectors in working electrodes. Generally, V_{oc} is considered the difference between the electronic Fermi level of the semiconductor used for the working electrode and the formal potential of the redox couples of the counter electrode. Therefore, because the semiconductor and the composition of the electrolyte were identical for all samples, the V_{oc} values of all the samples were nearly equal. Meanwhile, samples A and B exhibited lower J_{sc} values (6.35 and 11.45 mA/cm^2, respectively) than that of the nonpatterned FTO thin films (13.01 mA/cm^2). In addition, the ff values of sample A and sample B were also lower, at 36.99% and 40.30%, respectively. This is because, in the case of samples A and B, the FTO thin films functioning as electron collectors in the DSSCs had high sheet resistances despite having transmittances similar to that of the nonpatterned FTO thin films. Thus, the DSSCs fabricated using samples A and B displayed low PCEs (1.72% and 3.43%, respectively). However, sample C exhibits a higher PCE (6.58%) than did samples A and B, owing to its high J_{sc}, which was 15.02 mA/cm^2. The higher performances of these samples are attributable to the high surface areas and the low sheet resistances of the laser-patterned FTO thin films. In particular, improving the surface roughness with degrading the electrical properties increases the surface areas of the laser-patterned FTO thin films, enhancing their ability to be loaded with TiO_2 particles and

dyes. In addition, increasing the surface roughness increases J_{sc} and the PCE [14,18]. The PCE values of samples C-E

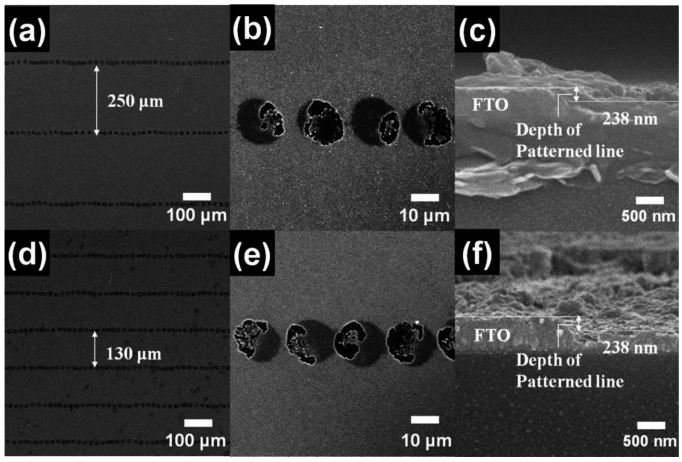

Fig. 4. Top-view and cross-sectional FESEM images of sample D (a-c) and sample E (d-f)

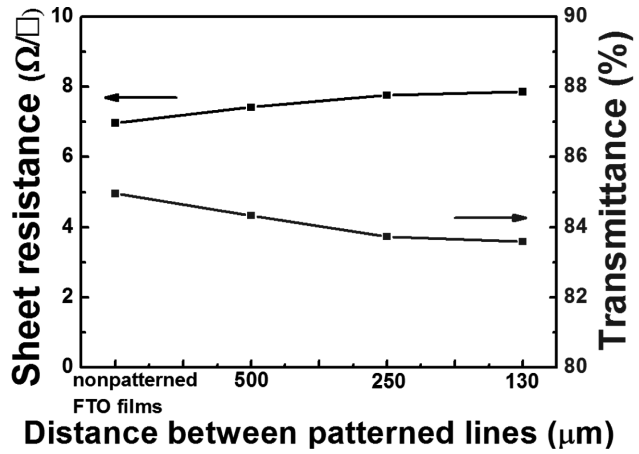

Fig. 5. Sheet resistances and optical transmissions at 550 nm of the samples depending on the distances between patterned lines

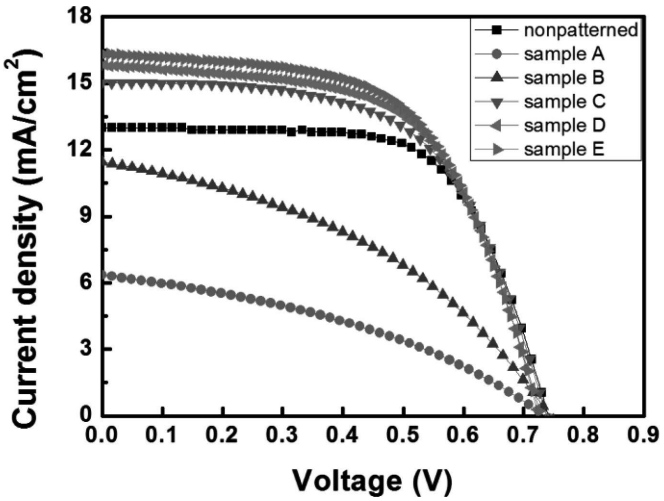

Fig. 6. Photocurrent density-voltage curves of DSSCs fabricated with nonpatterned FTO thin films and samples A-E

increased as the distance between patterned lines decreased. The values of J_{sc} were increased in particular, from 15.02 mA/cm^2 in sample C to 16.28 mA/cm^2 in sample E with the similar values of *ff*. This improvement is attributed to sample E having a large surface area than that of sample C, while exhibiting a comparably low sheet resistance. Since the distances between lines were smaller, the surface areas per unit area of the laser-patterned FTO thin films were higher. In addition, no electrical degradation was observed after the laser-etching process. Thus, more TiO_2 particles and dyes can be incorporated into the DSSCs, further improving the J_{sc} and PCE values. Therefore, sample E exhibit the highest short-circuit photocurrent density, a good fill factor, and the highest PCE (~7.00%) of all the samples. These properties were the result of the increase in the surface area of the FTO thin films after the laser-patterning process, while the sheet resistance of the films remained unchanged. Therefore, such materials show potential as promising current collector materials for high-performance DSSCs.

4. Conclusions

In conclusion, we employed a laser-patterning technique to modify the surface morphologies of FTO thin films to be used as current collectors in DSSCs. First, three laser power densities were used (samples A-C) while the distance between the patterned lines was kept fixed 500 μm. The samples patterned at high laser power densities showed poor sheet resistances compared to nonpatterned FTO thin film. This was because the increased depths of the patterned lines, resulting from the higher laser power densities, disturbed the smooth transfer of electrons along the FTO surface. However, sample C, produced using the lowest laser power density (1100 kW/mm^2) exhibited a large surface area without showing a decrease in electrical conductivity. In addition, we examined three different laser-patterned line spacings (samples C-E), which were etched using a fixed laser power density of 1100 kW/mm^2. Despite the fact that the distances between the patterned lines had little impact on the electrical and optical properties of the FTO films, the PCE values of DSSCs based in the films increased as the distance between the patterned lines was decreased. These results are attributed to the increase in the surface areas of the laser-patterned FTO thin films, while the low intrinsic sheet resistance of the FTO films remained unchanged. Of all of the samples examined, the DSSC based on sample E exhibited the highest PCE (~7.00%) owing to the sample being patterned using the lowest laser power density (1100 kW/mm^2) and having the narrowest gaps between its patterned lines (130 μm).

Acknowledgements

This work was supported by Grant No. 10046672 from the Ministry of Knowledge Economy (MKE) and R&D Program for Technology of Specialized Materials particularly designed for venture business funded by the Ministry of Knowledge Economy, Republic of Korea.

REFERENCES

[1] S.M. Wie, C.H. Hong, S.K. Oh, W.S. Cheong, Y.J. Yoon, J.S. Kwak, Ceram. Int. **40**, 11163 (2014).
[2] R.D. Slocombe, A. Porch, M. Pepper, P.P. Edwards, Energy Environ. Sci. **5**, 5387 (2012).
[3] M. Chen, Z.L. Pei, J. Gong, R.F. Huang, L.S. Wen, Mater. Sci. Eng. B **85**, 212 (2001).
[4] S. Calnan, A.N. Tiwari, Thin Solid Films **518**, 1839 (2010).
[5] C. Guillen, J. Herrero, Thin Solid Films **520**, 1 (2011).
[6] G. Hautier, A. Miglio, G. Ceder, G.M. Rignanese, X. Gonze, Nat. Commun. **4**, 2292 (2013).
[7] N. Noor, I.P. Parkin, J. Mater. Chem. C **1**, 984 (2013).
[8] M.H. Kim, H. Lee, Y.K. Jeoung, J. Kor. Powd. Met. Inst. **17**, 449 (2010).
[9] M.S. Kang, Y.S. Kang, J. Kor. Powd. Met. Inst. **12**, 7 (2005).
[10] B.J. Yoo, K.K. Kim, D.K. Lee, H.G. Kim, B.S. Kim, N.G. Park, M.J. Ko, J. Electrochem. Sci. Tech. **2**, 68 (2011).
[11] K.I. Jang, E. Hong, J.H. Kim, Kor. J. Chem. Eng. **29**, 356 (2012).
[12] F. Wang, N.K. Subba-Iyan, Q. Wang, C. Rochford, G. Xu, R. Lu, A. Elliot, F. D'Souze, R. Hui, J. Wu, Appl. Mater. Interfaces **4**, 1565 (2012).
[13] X. Zou, Y. Liu, C. Wei, Z. Huang, X. Meng, Int. J. Photoenergy **2014**, 890563 (2014).
[14] S.M. Kong, Y. Xiao, K.H. Kim, W.I. Lee, C.W. Chung, Thin Solid Films **519**, 3173 (2011).
[15] M.F. Chen, Y.P. Chen, W.T. Hsiao, Z.P. Gu, Key Eng. Mater. **364**, 315 (2008).
[16] H.K. Lin, W.C. Hsu, Appl. Surf. Sci. **308**, 58 (2014).
[17] M. Grätzel, J. Photochem. Photobiol. C **4**, 145 (2003).
[18] J.S. Kim, J.H. Kim, M.K. Lee, Nanotechnology **21**, 345203 (2010).

Received: 20 November 2014.